Neuroscience Research 191 (2023) 77–90

Contents lists available at ScienceDirect

Neuroscience Research

journal homepage: www.sciencedirect.com/journal/neuroscience-research

Neural mechanism of experience-dependent sensory gain control in *C. elegans*

Yosuke Ikejiri [a,b], Yuki Tanimoto [b,1], Kosuke Fujita [b,2], Fumie Hiramatsu [b,3], Shuhei J. Yamazaki [b], Yuto Endo [a,b], Yasushi Iwatani [c], Koichi Fujimoto [b], Koutarou D. Kimura [a,b,*]

[a] Department of Information and Basic Science, Graduate School of Science, Nagoya City University, Nagoya, Aichi 467-8501, Japan
[b] Department of Biological Sciences, Graduate School of Science, Osaka University, Toyonaka, Osaka 560-0043, Japan
[c] Department of Science and Technology, Graduate School of Science and Technology, Hirosaki University, Hirosaki, Aomori 036-8561, Japan

ARTICLE INFO

Keywords:
Gain control
Mathematical model
Sensory signaling
Calcium imaging
C. elegans

ABSTRACT

Animals' sensory systems adjust their responsiveness to environmental stimuli that vary greatly in their intensity. Here we report the neural mechanism of experience-dependent sensory adjustment, especially gain control, in the ASH nociceptive neurons in *Caenorhabditis elegans*. Using calcium imaging under gradual changes in stimulus intensity, we find that the ASH neurons of naive animals respond to concentration increases in a repulsive odor 2-nonanone regardless of the magnitude of the concentration increase. However, after preexposure to the odor, the ASH neurons exhibit significantly weak responses to a small gradual increase in odor concentration while their responses to a large gradual increase remain strong. Thus, preexposure changes the slope of stimulus–response relationships (*i.e.*, gain control). Behavioral analysis suggests that this gain control contributes to the preexposure-dependent enhancement of odor avoidance behavior. Mathematical analysis reveals that the ASH response consists of fast and slow components, and that the fast component is specifically suppressed by preexposure for the gain control. In addition, genetic analysis suggests that G protein signaling may be required for the regulation of fast component. We propose how prior experience dynamically and specifically modulates stimulus–response relationships in sensory neurons, eventually leading to adaptive modulation of behavior.

1. Introduction

Animals use their sensory organs to interpret stimuli from the external environment and to effectively survive and reproduce. The intensity of these stimuli can vary by a factor of 10^{10}, although the range of neuronal activity is generally limited to a factor of 10^2 (Shapley and Enroth-Cugell, 1984). Thus, animals need to adjust their range of neuronal activity in peripheral and central sensory systems according to stimulus intensity. Such regulation of neuronal responsiveness has been reported in visual, auditory, olfactory, mechanical, and nociceptive systems, in a variety of animal species ranging from invertebrates to vertebrates (Carew et al., 1971; Dragoi et al., 2000; Priebe and Ferster, 2002; Ulanovsky et al., 2003; Woolf and Ma, 2007; Root et al., 2008).

One type of neuronal response modulation is sensory gain control. Gain control refers to a modulation that changes the slope of stimulus–response relationships and is different from adaptation or sensitization, which decreases or increases the overall responsiveness (Fig. S1). Gain control has been reported to occur in the visual, auditory and somatosensory cortices of mammals and the olfactory circuit of *Drosophila*, and it is likely conserved across taxa (Ohzawa et al., 1982; Andersen et al., 1985; Chance et al., 2002; Olsen and Wilson, 2008; Anderson et al., 2017; Azimi et al., 2020). However, neuronal and/or molecular mechanisms underlying gain control, as well as the effect of gain control on sensory behavior, have not been sufficiently elucidated.

The nematode *Caenorhabditis elegans* has been widely used to study the mechanisms of sensory responses. The animals respond to various sensory stimuli, which are modulated by experience as learning, and the neurons and genes involved in these responses have also been identified

* Correspondence to: Graduate School of Science, Nagoya City University, Nagoya, 467-8501, Japan.
E-mail addresses: kokimura@nsc.nagoya-cu.ac.jp, kokimura-lab@umin.ac.jp (K.D. Kimura).
[1] Present address: RIKEN Center for Brain Science. Wako, Saitama 351-0106, Japan
[2] Present address: Department of Ophthalmology, Nagoya University Graduate School of Medicine. Nagoya, Aichi 466-8550, Japan
[3] Present address: Max Planck Institute for Neurobiology of Behavior (caesar), Bonn 53175, Germany

https://doi.org/10.1016/j.neures.2023.01.006
Received 3 November 2022; Received in revised form 15 January 2023; Accepted 16 January 2023
Available online 19 January 2023

(De Bono and Maricq, 2005; Bargmann, 2006; Sasakura and Mori, 2013; Ferkey et al., 2021). However, sensory gain control has been shown only in a few mutant strains of the animals (Kuhara et al., 2002; Saro et al., 2020), and it has not been clear whether and how sensory gain control contributes to the wild-type animals' sensory behavior, such as navigation under a chemical gradient.

C. elegans avoidance behavior to the odorant 2-nonanone is an ideal experimental paradigm to study the animals' sensory response and experience-dependent modulation. The animals avoid the odor, and this odor avoidance behavior is enhanced by preexposure to the odor for 1 h as a type of non-associative learning (Fig. 1A) (Bargmann et al., 1993; Kimura et al., 2010). We have found that olfactory AWB neuron pair and nociceptive ASH neuron pair respond to the odor decrease and increase, respectively. We have further revealed that slowly increasing activity in AWB and ASH neurons is dependent on L-type voltage-gated calcium channel (VGCC) EGL-19 and that the slow activity can be modeled by a leaky integrator equation (Fig. 1B and C; Tanimoto et al., 2017). Interestingly, we have also found that the ASH response to a small odor increase is reduced by odor preexposure, indicating an experience-dependent modulation of its activity, although its detail has not been revealed (Yamazaki et al., 2019). ASH neurons are considered as a simple model for polymodal nociceptive neurons evolutionarily conserved from worms to mammals (Kaplan and Horvitz, 1993). Thus, analyzing the experience-dependent changes in ASH response to 2-nonanone will be ideal to address questions at the levels of behavior, neural activity, and molecules.

In this study, we show that sensory gain control occurs in ASH sensory neurons of *C. elegans* for efficient odor avoidance by preexposure to

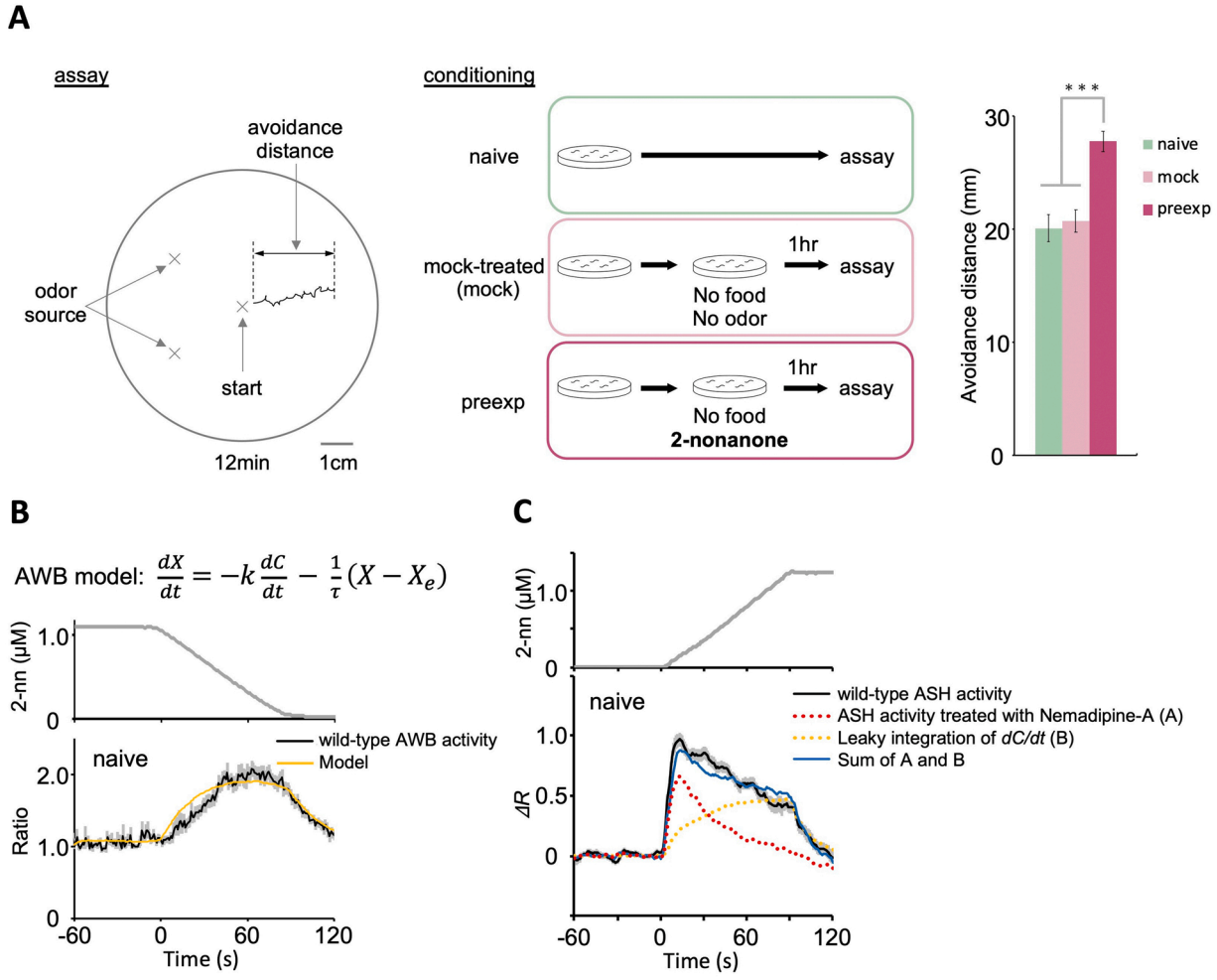

Fig. 1. *C. elegans* avoidance behavior to the odorant 2-nonanone and neural responses related this behavior. **A,** Preexposure-dependent enhancement of odor avoidance behavior. (left) Example of an animal's trajectory tracked during 12 min of 2-nonanone avoidance assay. (middle) The three conditions for 2-nonanone avoidance assay. (right) Result of 2-nonanone avoidance assay, where the average avoidance distance ± standard error in each condition is shown (n = 47, 45, 44 in naive, mock-treated, and preexposed conditions, respectively). Compared to control (*i.e.,* naive and mock-treated) animals, preexposed animals exhibit significantly longer avoidance distances. * ** $p < 0.001$ (Kruskal-Wallis test with *post hoc* Steel-Dwass test). **B,** AWB response to a constant gradual decrease in 2-nonanone concentration. When a constant odor decrease (upper panel) is presented, AWB neurons in naive wild-type animals exhibit a gradually increasing response (black solid line in lower panel), which is mainly dependent on L-type VGCC EGL-19 and can be approximated by the leaky integration equation (top and yellow line in lower panel). The details of leaky integration equation are described in Materials and Methods. **C,** ASH response to a constant gradual increase in 2-nonanone concentration. When a simple gradual odor increase (upper panel; odor gradient #1) is presented, ASH neurons in naive wild-type animals exhibit a fast and relatively constant response (black solid line in lower panel). In contrast, when wild-type animals are treated with Nemadipine-A, a specific antagonist for EGL-19, ASH exhibits a fast and transient response (red dotted line in lower panel). Interestingly, when the transient response and the calculated leaky integration of time-differential of odor concentration mediated by the EGL-19 (yellow dotted line) are added (blue solid line), the added result nicely reproduces the actual ASH response. For panel C, instead of the ratio (GCaMP/mCherry), Δ*R* (ratio - baseline) was used because two different groups of wild-type ASH responses (untreated *versus* NemA-treated) were compared in this panel. Panels B and C are reproduced from the previous studies with some modifications (Tanimoto et al., 2017); the solid lines and associated shadows are the average values and their standard errors, respectively (For interpretation of the references to color in this figure legend, the reader is referred to the web version of this article).

2-nonanone *via* specific suppression of one of its activity components. We find that preexposure changes the slope of the stimulus–response relationships, *i.e.* gain control, and that this experience-dependent modulation of sensory activity is consistent with the changes in the animals' behavioral responses. On mathematical modeling, ASH response is well fitted as the sum of fast and slow components, and the preexposure experience suppresses the fast component specifically. Furthermore, genetic analysis suggests that G protein signaling may regulate this suppression. Thus, our results demonstrate how experience-dependent modulation of stimulus–response relationships occurs in a sensory neuron and how it leads to changes in behavioral responses.

2. Materials and methods

2.1. Strains

The techniques used to culture and handle *C. elegans* were essentially as described previously (Brenner, 1974). *C. elegans* wild-type Bristol strain N2, JC2628 *osm-9(ky10) ocr-2(ak47)*, RB1780 *rgs-3(ok2288)*, MT1073 *egl-4(n478)*, DR1089 *unc-77(e625)*, and VC550 *tag-180 (ok779)*, were obtained from the Caenorhabditis Genetics Center (University of Minnesota, USA). In all the behavioral and physiological experiments, we used young adult hermaphrodites.

2.2. Calcium imaging by OSB2 system

Calcium imaging of ASH sensory neurons was performed as previously reported with some modifications (Tanimoto et al., 2017; Yamazaki et al., 2019; Tanimoto and Kimura, 2021). In brief, transgenic lines expressing GCaMP3 (Tian et al., 2009) and mCherry (Shaner et al., 2004) in ASH neurons of wild-type N2 background (20 ng/μl of *sra-6p*::GCaMP3, 20 ng/μl of *sra-6p*::mCherry, 10 ng/μl of *lin-44p*::GFP, 50 ng/μl of *Pvu*II-cut N2 genomic DNA; KDK70034 and KDK70072) were placed on NGM plates and observed under our original microscope system, OSB2. To measure the neural activity of multiple animals in a single observation, the transgenic animals were immobilized using levamisole, an agonist to the acetylcholine receptor (Lewis et al., 1980); ASH response is not affected by levamisole treatment (Tanimoto et al., 2017). If possible, neural activity was measured from the left and right ASH neurons in an animal. Each experimental condition was tested multiple times per day, which was repeated for 2–3 days in total. Experimental conditions, such as strains, odor stimuli and conditioning of the animals, were randomly set for each day.

For odor stimulation, we delivered a mixture of 2-nonanone and air at a total of 8 mm/min and created a temporally changing gradient of odor concentration by changing the ratio of 2-nonanone to air. We measured this gradient using a custom-made semiconductor sensor at the tube end before and after performing the calcium imaging experiments on each day. The sensor was calibrated every day with 0.5, 1, 2 and 4 μM concentrations (Tanimoto and Kimura, 2021).

We divided the fluorescent signals of GCaMP3 and mCherry through a dual-wavelength measurement optical system, W-VIEW (Hamamatsu Photonics), and captured their fluorescence images using an EM-CCD camera (ImagEM, Hamamatsu Photonics) at a sampling rate of 10 Hz. After subtracting the background, we extracted the fluorescence intensity of the cell body using ImageJ (NIH) and used their ratio (GCaMP/mCherry) as the data.

2.3. Conditioning of the animals

Calcium imaging of ASH was performed using OSB2 under the following three conditions as previously described (Kimura et al., 2010; Yamazoe-Umemoto et al., 2015). (1) Naive: the animals were cultivated on 6 cm NGM plates with OP50 provided as food, and were then washed briefly with NGM buffer and measured; (2) Preexp: the animals were preexposed to 0.6 μl of 15% 2-nonanone (diluted in ethanol) for 1 h on a 6 cm NGM plate without food; and (3) Mock-treated: the animals were preexposed to ethanol in the same way as the preexp condition. The mock-treated condition is a control that shows that starvation itself does not affect the response to 2-nonanone.

2.4. Data analysis and statistical analysis

After the data acquisition, animals with too weak intensity of basal mCherry or GCaMP3 fluorescence were excluded because of the difficulty in tracking. To exclude noise, frames in which the GCaMP/mCherry ratio was in the top 1% and bottom 1% of the total were removed. Statistical analyses were performed using the Kruskal-Wallis test with a *post-hoc* Steel-Dwass test using R (ver. 3.2.3, The R Project). In the figure, * indicates $p < 0.05$, * * indicates $p < 0.01$, and * ** indicates $p < 0.001$. Scatter plots represent median ± quartiles and other graphs represent the mean ± standard error. We chose the sample size based on a large scale behavioral analysis of *C. elegans* (Yemini et al., 2013).

2.5. Mathematical modeling of AWB-like responses by leaky integration

Mathematical modeling of AWB-like responses was described in our previous work (Fig. 1B; Tanimoto et al., 2017). In brief, the activity of AWB neurons, which respond to decreases in 2-nonanone concentration, is well fitted with the following leaky integrator equation:

$$\frac{dX(t)}{dt} = I - \frac{1}{\tau}(X(t) - X_e) \quad (1)$$

$$I = -k\frac{dC(t)}{dt}$$

where $X(t)$ is the measured fluorescence signal of the neuron (GCaMP/mCherry), I is the input, X_e is the basal calcium level in the steady state, k and $1/\tau$ are the parameters, and $C(t)$ is the measured odor concentration. The model parameters k, $1/\tau$, and X_e were determined by the simple least-squares method (Excel solver). Eq. (1) indicates that the neuronal response $X(t)$ increases according to the input (negative $dC(t)/dt$) and reduces ("leaks") according to the $X(t)$ itself and returns to the steady state X_e. For example, when an animal experiences a constant decrease in odor concentration, the constant decrease is transformed to a constant depolarization, and it causes constant calcium influx *via* L-type VGCC EGL-19, and the calcium concentration reduces according to its total amount possibly *via* leak channel(s) (Tanimoto et al., 2017). Since AWB neurons respond only to decreases in odor concentration, zero is substituted to $dC(t)/dt$ when $dC(t)/dt$ is positive in Eq. (1). This AWB activity was essentially abolished by treatment of animals with Nemadipine-A (NemA), the antagonist of *C. elegans* L-type VGCC (Kwok et al., 2006) or by *egl-19* mutation, indicating that the AWB activity is mainly mediated by the L-type VGCC homolog EGL-19.

In NemA-treated animals, ASH neurons are rapidly activated at the beginning of the odor-increasing phase but soon inactivated gradually even though the odor concentration kept increasing (red dotted line in Fig. 1C). When we assumed that the NemA-treatment suppressed AWB-like leaky integration activity (yellow dotted line in Fig. 1C), the sum of the remaining and the suppressed activities (blue solid line in Fig. 1C) nicely resembled the measured ASH activity (black solid line in Fig. 1C). We call the transient and gradual activities the fast and slow components, respectively (Tanimoto et al., 2017).

2.6. The first and second differential model of ASH responses

We extended the previous model Eq. (1) by introducing the second-order time differential of input C representing the fast component:

$$\frac{dX(t)}{dt} = k_1\frac{dC(t)}{dt} + k_2\frac{d^2C(t)}{dt^2} - \frac{1}{\tau}(X(t) - X_e) \quad (2)$$

where $X(t)$ is the measured ASH signal, X_e is the basal calcium level, and k_1, k_2 and $1/\tau$ are parameters for the first- and second-order time differential and the leaky part, respectively. The parameters k_1, k_2, $1/\tau$, and X_e were determined by the simple least-squares method for each odor stimulus. $dC(t)/dt$ and $d^2C(t)/dt^2$ were calculated using the central difference scheme. Since ASH neurons respond only to increases in odor concentration (Tanimoto et al., 2017), zero is substituted to $dC(t)/dt$ or $d^2C(t)/dt^2$ when $dC(t)/dt$ or $d^2C(t)/dt^2$ is negative in Eq. (2).

The first and second differential model Eq. (2) is further extended on the terms of the second-order time-differential and X_e:

$$\frac{dX(t)}{dt} = k_1\frac{dC(t)}{dt} + \Phi\left(k_2\frac{d^2C(t)}{dt^2}\right) - \frac{1}{\tau}(X(t) - X_e(t)), \quad (3)$$

where $\Phi(x)$ is the saturation function as the following equation:

$$\Phi(x) = \left\{ \begin{array}{c} 0.14, \text{ if } x > 0.14 \\ x, \text{ if } x \le 0.14 \end{array} \right\} \quad (4)$$

This saturation function is introduced to prevent the parameters from becoming too large when the dC/dt approaches zero. 0.14 was arbitrary determined.

$X_e(t)$ changes over time as follows:

$$X_e(t) = \left\{ \begin{array}{c} b_1, \text{ if } t < t_1 \\ \frac{b_2 - b_1}{t_2 - t_1}(t - t_1) + b_1, \text{ if } t_1 \le t \le t_2 \\ b_2, \text{ if } t_2 < t \end{array} \right\} \quad (5)$$

where t_1 is the time at the start of the first odor increase phase, and t_2 is the time at the end of the first odor increase phase. The parameters b_1 and b_2 were determined by the simple least-squares method with the actual ASH response during 30 s until 10 s before the start of the first odor increase phase (t_1) and 1 min after the first odor stimulus (t_2), respectively, in each condition (Table 3). Eq. (5) was introduced because the basal calcium level changed after the first odor stimulus. This equation indicates that the steady-state calcium concentration could be affected by recent experience with the odor stimulus.

In terms of parameters in Eq. (3), we plotted the relationships among parameters (k_1, k_2, and $1/\tau$) and various aspects of odor inputs (average, maximum, or accumulation of C, dC/dt, and d^2C/dt^2) and fitted the relationships to the logarithmic function ($y = f\ln(x) + g$) of the odor inputs (Excel solver) (Fig. 6 A and Fig. S6); fitting of k_1 and $1/\tau$ to linear functions ($y = h\ x + i$) of the odor inputs was worsened (Table 2). We chose the aspect of odor input with the smallest or the second smallest residual sum of squares, and the logarithmic functions of our chosen aspect for k_1 and $1/\tau$ were similar between naive, mock-treated and preexposed conditions. Thus we further optimized the parameters f and g manually such that they were the same for all three conditions (Fig. 6A).

As a lower threshold for $1/\tau$, the following function is introduced:

$$\frac{1}{\tau} = \left\{ \begin{array}{c} 0.02\ln(x) + 0.11, \text{ if } x > 0.1 \\ 0.02\ln(0.1) + 0.11, \text{ if } x \le 0.1 \end{array} \right\} \quad (6)$$

where x denotes $d^2C(t)/dt^2$. This function is introduced to prevent $1/\tau$ from becoming too small when the increase in odor concentration approaches zero (Fig. 6A). 0.1 was arbitrary determined.

2.7. Evaluation of the mathematical model

The Bayesian information criterion (BIC) (Schwarz, 1978) was used to assess the fit of the data using a mathematical model. The smaller the BIC value, the better is the model fit. In BIC, the goodness of fit for the model, including a penalty term to prevent overfitting, is given by the following equation:

$$\mathrm{BIC} = N\ln\left(\frac{RSS}{N}\right) + M\ln(N) \quad (7)$$

where N is the number of frames used for the fitting, RSS is the sum of the squared residuals between the model and the actual response, and M is the number of free parameters used in the model. $M = 2$ for the original simple time-differential model (Fig. 5A and S3A) because of k and X_e, $M = 3$ for the model with the leaky integration of only first- or second-order time-differential (Fig. 5B, C and S3B, C) because of k_1 or k_2 and $1/\tau$ and X_e, $M = 4$ for the first and second differential model (Fig. 4B) because of k_1, k_2, $1/\tau$ and X_e, and $M = 12$ for the first and second differential model with stimulus-dependent parameters (Fig. 6B) because there were two parameters each in the stimulus-dependent parameters k_1, k_2, and $1/\tau$, four parameters in $X_e(t)$, one parameter in $\Phi(x)$, and one parameter in lower threshold for $1/\tau$.

2.8. Behavioral analysis

Trajectories obtained by a high-resolution USB camera (DMK72AUC02; The Imaging Source, United States) during 2-nonanone avoidance behavior were clustered using the previously reported STEFTR method (Yamazaki et al., 2019). In brief, clustering was performed using variances of temporal changes in bearing, and the cluster with the smallest variances of temporal changes in bearing was classified as "run" (a period of relatively long straight movement), while the other clusters were classified as "pirouette" (a period of short movements interrupted by frequent reversals and turns) categories. This classification of "run" and "pirouette" was more than 90% consistent with the previous one based on the durations of straight migration: Essentially, if a worm's migration was not interrupted by an angle change larger than 90° /s for ≥ 14 s, the migration was classified as a run; turns and shorter migrations were classified as pirouettes (Yamazoe-Umemoto et al., 2015). Then, the change in the odor concentration sensed during the run was calculated according to an odor gradient model based on the measured odor concentrations (Yamazoe-Umemoto et al., 2015). The behavioral data have already been used previously (Yamazaki et al., 2019), and re-analyzed in this study.

3. Results

3.1. Sensory gain control in ASH neurons caused by odor preexposure

To reveal how experience changes the activities of sensory neurons under conditions of physiologically meaningful odor stimuli, we investigated ASH activities before and after preexposure to 2-nonanone. Our previous quantitative behavioral analysis revealed that *C. elegans* senses approximately 5–20 nM/s concentration changes during 2-nonanone avoidance behavior (Yamazoe-Umemoto et al., 2015). Therefore, in this experiment, we used three types of stimuli in a series of odor stimulations: (1) a minimum increase that could be provided stably by our original microscope system OSB2 (3 nM/s) (Tanimoto et al., 2017); (2) a maximum increase sensed during the behavioral experiment (20 nM/s); and (3) an even larger increase (40 nM/s). We measured the ASH responses to these stimuli under three different conditions with prior treatments: naive, mock-treated, and preexposed (Fig. 1A).

In the naive condition, the ASH response to 3 nM/s started to increase immediately after the onset of odor increase, quickly reached close to the maximum value, and the magnitude of the response was sustained during the odor increase (Fig. 2A). When the odor began to decrease, the response also decreased, and when the odor concentration returned to zero, the ASH response returned to a basal level. The ASH responses to 20 and 40 nM/s odor increases were essentially similar to the response to 3 nM/s in magnitude and pattern. The results of the mock-treated condition were similar to those of the naive animals. In

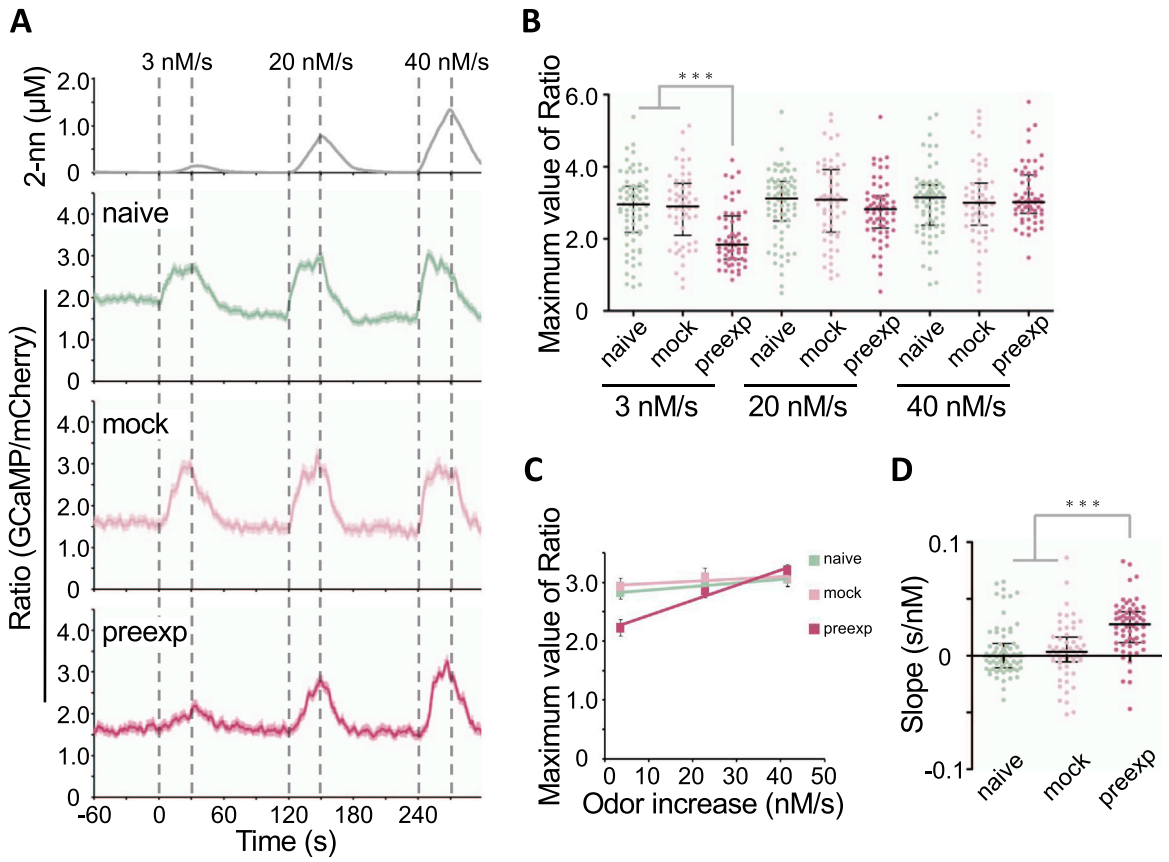

Fig. 2. Preexposure to the repulsive odor 2-nonanone causes the sensory gain control in ASH neurons. **A,** ASH responses to three consecutive stimuli (3, 20, and 40 nM/s; top) in the three conditions. In the naive (green) and mock-treated (pale red) conditions, the responses were always large regardless of the stimulus intensity. However, in the preexposure condition (dark red), the responses were smaller for small stimuli and larger for large stimuli. The solid lines and associated shadows are the average values and their standard errors, respectively (n = 71, 57, 61 in naive, mock-treated, and preexposed conditions, respectively). The gray dotted lines indicate the onset and end of the odor increase phase. **B,** Scatter plot of the maximum values of ASH response (shown in panel A) to each stimulus. * ** $p < 0.001$ (Kruskal-Wallis test with *post hoc* Steel-Dwass test). **C,** Correlation between the rate of odor concentration increase and the maximum value of ASH response. The mean ± standard error of ASH maximum values in panel B and its linear approximation are shown. **D,** Scatter plot of the slope of the response. Each slope was calculated by linear approximation of maximum values of ASH responses of an animal to the three stimuli (3, 20, and 40 nM/s). * ** $p < 0.001$ (Kruskal-Wallis test with *post hoc* Steel-Dwass test). The statistical details are described in Supplementary Table 1 (For interpretation of the references to color in this figure legend, the reader is referred to the web version of this article).

summary, the magnitude of the response was always constant in naive and mock-treated conditions, regardless of the magnitude of the odor increase.

In the preexposed condition, unlike naive and mock-treated animals, ASH did not respond much to the 3 nM/s increase. Its maximum value was substantially smaller than those in the naive and the mock-treated animals, and the activity slowly increased and reached the maximum value at the end of the odor-increasing phase (Fig. 2A); this smaller response after preexposure is consistent with our previous finding (Yamazaki et al., 2019). Unexpectedly, however, we newly found that ASH responded strongly to the 20 and 40 nM/s increases even after preexposure, and the magnitude of the response increased according to the magnitude of the odor increase (Fig. 2A).

In terms of the maximum response to each odor increase, there was no significant difference in the responses to 20 and 40 nM/s, but the response to 3 nM/s was significantly smaller in the preexposed animals than in the naive and mock-treated animals (Fig. 2B). The linear approximation of the average responses to each odor increase did not change much in the naive and mock-treated conditions, but was positive in the preexposed condition (Fig. 2 C). Furthermore, by calculating the slope of each animal's response to the 3, 20, and 40 nM/s stimuli, we found that the slopes of the preexposed response were significantly larger than those of the naive and mock-treated responses (Fig. 2D). Thus, the slope of stimulus–response relationships of ASH neurons changes because of preexposure to the odor, not adaptation or sensitization, which is an overall increase or decrease of the relationships without changes in its slope (Fig. S1). In other words, gain control occurs in ASH neurons because of preexposure to the odor.

3.2. *Behavioral significance of ASH gain control by preexposure*

Next, we investigated whether the ASH gain control after preexposure could explain the enhanced 2-nonanone avoidance behavior (Kimura et al., 2010). In previous studies, we found that the odor avoidance behavior consists of two behavioral states: (1) run, a period of long straight movement, and (2) pirouette, a period of repeated short movements with frequent directional changes (Fig. S2) (Pierce--Shimomura et al., 1999; Kimura et al., 2010). Since ASH responds to the odor increase to cause pirouettes (Tanimoto et al., 2017), a simple scenario would be that ASH sensitivity increases to make the animal avoid 2-nonanone sooner after preexposure. However, our results indicate that ASH after preexposure is less sensitive when the increase in odor concentration was small (Fig. 2A).

To understand how changes in ASH response as gain control affect odor avoidance behavior, we calculated time-course changes in odor concentration that each animal sensed during the odor avoidance. This calculation was according to the model of 2-nonanone evaporation and diffusion, which is based on the actual measurement of the local odor

concentration in the air phase of the plate (Tanimoto et al., 2017). We then analyzed the reverse correlations between odor concentration changes and behavioral aspects of the animals.

We found that the change in odor concentration upon initiation of the pirouette phase was almost zero in the naive and mock-treated conditions, but was positive in the preexposed condition (Fig. 3A). This suggests that naive and mock-treated animals initiated pirouettes in response to very small increases in odor concentration, while the preexposed animals responded only to larger increases. This is consistent with our results on the ASH response, which is very sensitive to a small odor increase in naive and mock-treated conditions, but less sensitive in the preexposed condition (Fig. 2). This change can explain the enhanced odor avoidance behavior by the animals after odor preexposure (Fig. 3B) (see Discussion).

3.3. Modeling the experience-dependent gain control in ASH activity

In order to obtain quantitative insights into the mechanism of gain control caused by preexposure, we performed mathematical modeling of the ASH response. In our previous study, the AWB response to a simple

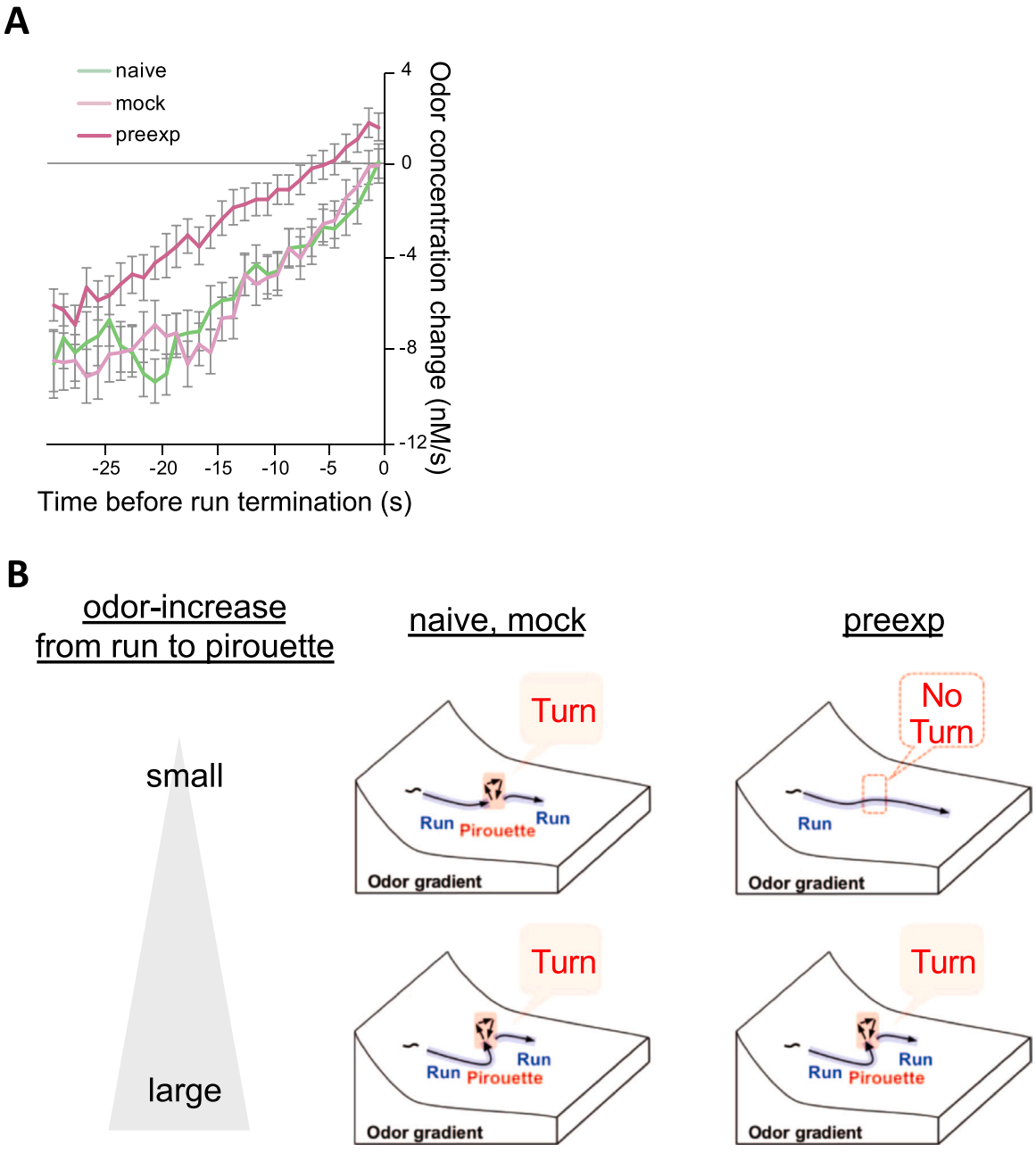

Fig. 3. Experience-dependent modulation of the odor avoidance behavior due to ASH gain control. **A,** Time-course changes of odor concentration that the animals sensed before the initiation of a pirouette. The odor concentrations that each animal sensed 30 s before the initiation were ensemble-averaged. The average values ± standard error of naive, mock-treated, and preexposed animals are shown in green, pale red and dark red, respectively (n = 50 in all conditions). In the naive and mock-treated animals, the transition from run to pirouette on average occurred when the average value of odor concentration change became close to zero, whereas the transition occurred several seconds after the animals started sensing increases in the odor concentration in the preexposed condition. **B,** A model relationship between odor concentration change and behavioral response during odor avoidance behavior. An efficient avoidance behavior is accomplished by suppressing the response to a slight odor increase. A part of this figure has been published previously (Yamazaki et al., 2019) (For interpretation of the references to color in this figure legend, the reader is referred to the web version of this article).

gradual odor decrease is modeled by the leaky integration of time-differential (dC/dt) of odor concentration (C) (see Fig. 1B and Eq. (1) in Materials and Methods), and the ASH response to the simple gradual odor increase (odor gradient #1 used in Fig. 1C) was modeled by simple time-differential of odor concentration (Tanimoto et al., 2017). However, the simple time-differential model did not sufficiently reproduce the ASH response to the series of three odor stimulations (odor gradient #2 used in Fig. 2A), especially in the later phase of each odor stimulus and in the preexposed condition (Fig. S3A).

Because our pharmacological study suggested that the ASH response to the odor gradient #1 consists of fast and slow components, and the slow component was modeled by the leaky integration of time-differential of odor concentration (Fig. 1C), we sought to model the fast component of ASH response mathematically. The fast component started to increase at the onset of odor concentration increase, and soon it started to decrease even when the odor concentration continued to increase (red dotted line in Fig. 1C). This time course of the fast component can be approximated by a leaky integration of the second-order time-differential (d^2C/dt^2) of the odor concentration (vertical gray bar and red line in "d^2C/dt^2" panel in Fig. 4A). We extended the

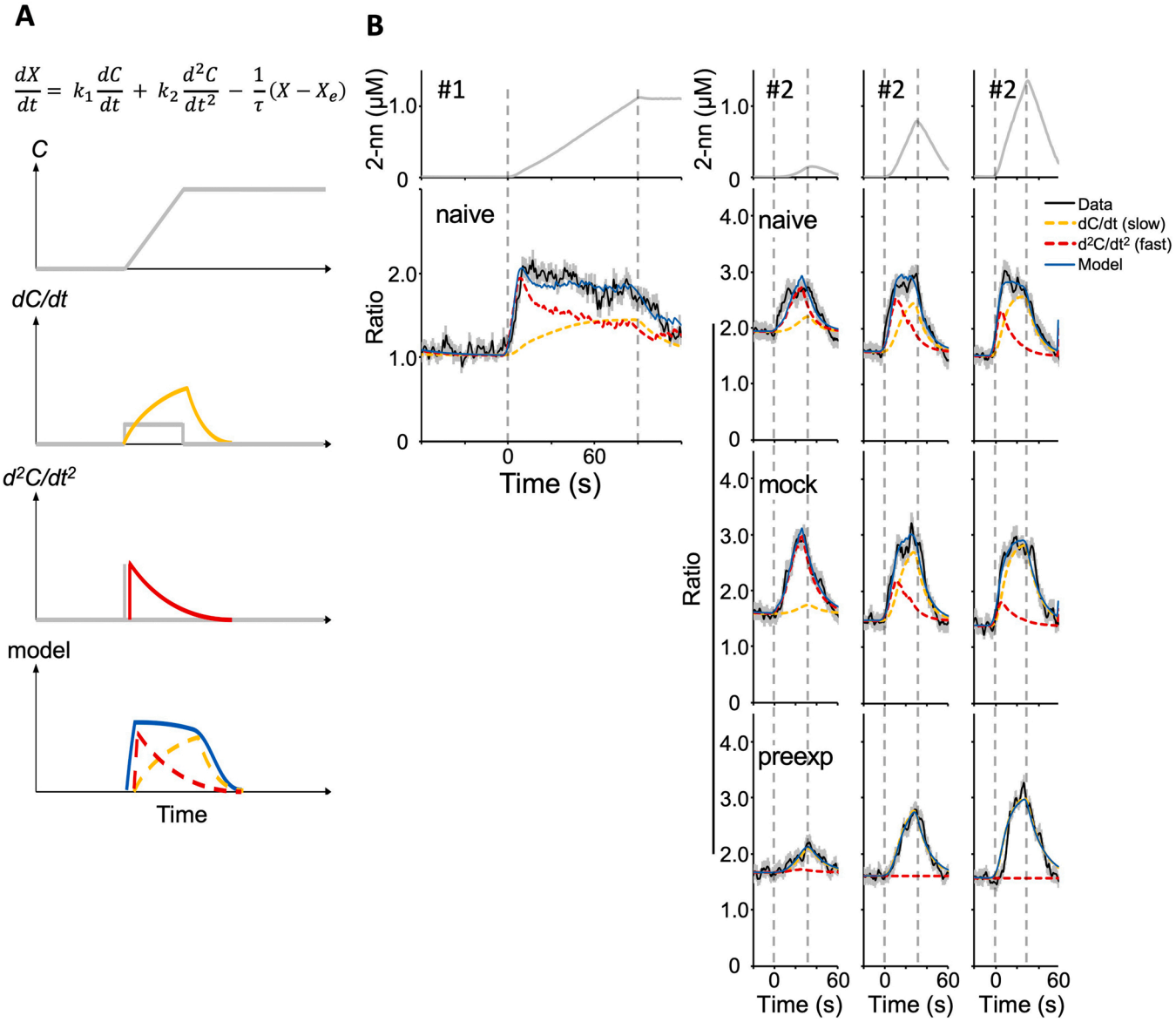

Fig. 4. Mathematical model of wild-type ASH response independently fitted to a single odor stimulus. **A,** Schematic drawing of a mathematical model of ASH response. Equation of the first and second differential model is shown at the top. Also shown are the time course of a simple gradual odor concentration increase (top panel), first-order time-differential of odor concentration and its leaky integration (gray rectangle and yellow line, respectively, in the second panel), second-order time-differential of the odor concentration and its leaky integration (gray vertical bar and red line, respectively, in the third panel; negative value of second-order time-differential is not calculated), and the sum of leaky integration of first- and second-order time-differentials (blue solid, yellow dashed and red dashed lines, respectively, in the bottom panel). **B,** The results of fitting the ASH response to the simple gradual odor increase used in the previous study (left; odor gradient #1, n = 39) and independent fitting to each of three consecutive odor stimuli used in Fig. 2A (right; odor gradient #2, n = 71, 57, 61 in naive, mock-treated, and preexposed conditions, respectively). The top panels exhibit each odor concentration change, and lower panels exhibit ASH responses to each stimulus of animals with different conditioning (naive, mock-treated or preexposed). The black line and the associated gray area are the average ASH responses and their standard errors, the blue line is the model, the yellow and red dashed lines are the first- and second-order components in the model, respectively. The gray dotted line indicates the onset and end of the odor increase phase. Note that in the preexposed condition, the first-order component (yellow) and the sum (blue) almost completely overlapped because the contribution of second-order component (red) was very small (For interpretation of the references to color in this figure legend, the reader is referred to the web version of this article).

model, hereafter referred to as "first and second differential model", where the ASH response itself is represented by a leaky integration of the sum of both the first- and second-order time-differentials of the odor concentration (Fig. 4A; Eq. (2) in Materials and Methods).

We examined whether the first and second differential model could reproduce the ASH responses to odor gradients #1 and #2. By determining the model parameters to the odor gradient #1 and to each odor stimulus in odor gradient #2 independently, the model reproduced the ASH activities well in most of the conditions (blue lines in Fig. 4B). Interestingly, the contribution of the fast component in ASH activities was substantially lower in preexposed than in naive and mock-treated conditions (red lines in right panels in Fig. 4B), suggesting that the fast component is specifically suppressed by the preexposure (see below).

To test the optimality of the first and second differential model, we compared the goodness of fit among the first and second differential model and three other models: the original simple time-differential model, and leaky integration of only first- or second-order time-differential models (Fig. 5 and S3). By calculating the Bayesian Information Criterion (BIC) (Schwarz, 1978) for each model, we found that the first and second differential model had the best or close-to-the-best goodness of fit in all naive and mock-treated conditions (Table 1), demonstrating the optimality of the model for these conditions. In the preexposed condition, the leaky integration of first-order time-differential model had the best fit, consistent with the suppression of the fast (second-order time-differential) component in ASH activity (Fig. 4B right).

The contributions of the fast and slow components exhibited remarkable differences for every odor gradient #2. For example, in naive and mock-treated conditions, the fast component became significantly smaller when odor concentration increased more rapidly (compare the response to the first odor stimulus to the ones to the second and third odor stimuli) (Fig. 4B right and Fig. S4). Consistently, when these parameters were uniquely determined for all the odor stimuli, the model did not accurately reproduce the ASH responses to odor gradient #2 (Fig. S5). These results suggest that the parameters depend on some aspects of the stimuli, such as the odor concentration and/or its changing velocity.

To test whether and how the parameters depend on aspects of stimuli, we plotted the relationships between the parameters and multiple aspects of the odor stimuli. We found that each parameter approximately follows a logarithmic function of the stimulus intensity (Fig. S6 and Table 2). Interestingly, in the well-fitted cases (red rectangles in Fig. S6), this function of the slow component (k_1) and the leaky part ($1/\tau$) were similar among naive, mock-treated and preexposed conditions, although that of the fast component (k_2) was much lower for preexposed than for naive and mock-treated conditions. When we further introduced this stimulus-intensity dependency into the first and second differential model (Eqs. (3)–(5) in Materials and Methods and Table 3), the model unifyingly reproduced the ASH responses to odor gradients #1 and #2 as well as their gain control-dependent changes (Fig. 6A and B). These results suggest that the contributions of fast and slow components and the leak of ASH response depend on the function of the odor stimulus intensity and that the fast component is further suppressed after odor preexposure for the gain control. The differences in the relationships between stimuli aspects and each parameter may reflect the regulatory mechanisms of fast and slow components and the leak activity (see Discussion).

3.4. Genetic analysis of the ASH response

Finally, we searched for genes possibly involved in the fast component of ASH responses. We hypothesized that the mutants of such genes would exhibit the slow component-like response in naive or mock-treated (*i.e.*, control) conditions.

We first analyzed mutants of cation channels. *osm-9* and *ocr-2* are the homologs of TRPV cation channels and known to function in ASH neurons for depolarization caused by sensory stimuli (Colbert et al., 1997; Tobin et al., 2002) although their physiological role in 2-nonanone sensation has not been revealed. *osm-9 ocr-2* double mutants exhibited substantially no response (Fig. 7A), suggesting that they are also required for sensory depolarization caused by 2-nonanone. The L-type VGCC subunit α1 EGL-19 is responsible for the slow component, although loss-of-function mutations in N- and T- types of VGCC subunit α1, *unc-2* and *cca-1* respectively, did not affect ASH response to the odor (Tanimoto et al., 2017). In this study we tested the homologs of a VGCC auxiliary subunit α2δ2 and a sodium leak channel, *tag-180* and *unc-77*,

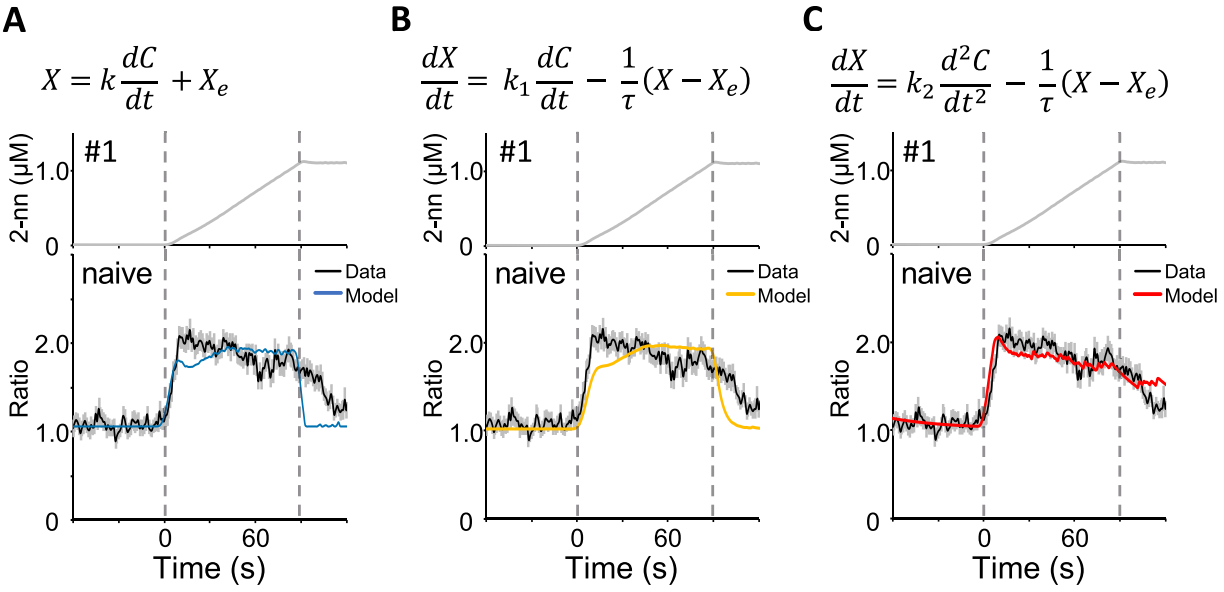

Fig. 5. Independent fitting of the wild-type ASH response to the odor gradient #1 with other models. **A,** Equation and the fitting results of the ASH response with the original simple time-differential model. **B,** Equation and the fitting results of the ASH response with the leaky integration of first-order time-differential model. **C,** Equation and the fitting results of the ASH response with the leaky integration of second-order time-differential model. In each panel, the black line indicates the actual ASH response (same with Fig. 4B left) and the colored line indicates the model, respectively. The gray dotted line indicates the onset and end of the odor increase phase (For interpretation of the references to color in this figure legend, the reader is referred to the web version of this article).

Table 1
Summary of comparing BIC values among mathematical models.

Odor gradient	#1	3 nM/s increase in #2			20 nM/s increase in #2			40 nM/s increase in #2		
Condition	Naive	Naive	Mock-treated	Preexp	Naive	Mock-treated	Preexp	Naive	Mock-treated	Preexp
$X = k\frac{dC}{dt} + X_e$	-557.3	-216.9	-195.0	-278.5	-153.5	-125.8	-140.8	-158.9	-92.5	-68.8
$\frac{dX}{dt} = k_1\frac{dC}{dt} - \frac{1}{\tau}(X - X_e)$	-559.9	-240.4	-217.7	**-423.4**	-205.0	-233.8	**-379.2**	-235.6	-260.8	**-261.5**
$\frac{dX}{dt} = k_2\frac{d^2C}{dt^2} - \frac{1}{\tau}(X - X_e)$	-741.1	**-287.6**	**-368.6**	-373.8	-253.5	-211.6	-211.3	-224.4	-159.4	-109.7
$\frac{dX}{dt} = k_1\frac{dC}{dt} + k_2\frac{d^2C}{dt^2} - \frac{1}{\tau}(X - X_e)$	**-769.6**	-286.5	-366.7	-420.5	**-301.2**	**-298.1**	-374.8	**-336.3**	**-289.0**	-257.1

BIC values were calculated independently for each odor stimulus. The smallest BIC values under each condition are indicated in bold.

Table 2
Comparison of BIC values for linear and logarithmic approximation of stimulus-dependent parameters.

Odor gradient	#1	#2		
Condition	Naive	Naive	Mock-treated	Preexp
Linear approximation	-539.2	-899.6	-1009	-682.0
Logarithmic approximation	**-778.4**	**-1135**	**-1116**	**-966.9**

The smallest BIC values under each condition are indicated in bold. In all the conditions, the model with a logarithmic approximation has a better BIC value than the model with a linear approximation.

respectively (Yeh et al., 2008; Lainé et al., 2011). Both of the mutant strains exhibited wild-type-like responses that were properly fitted with the ASH model (Fig. 7A), indicating that these genes are not involved in the ASH response either.

We then analyzed other candidates that have been known to be involved in modulation of sensory neuronal activity in *C. elegans*: *egl-4* (cyclic GMP-dependent protein kinase: PKG), and *rgs-3* (regulator of G protein signaling: RGS) (L'Etoile et al., 2002; Ferkey et al., 2007). The ASH responses of *egl-4* and *rgs-3* mutants in the control condition were substantially suppressed (black lines in Fig. 7A). Remarkably, the ASH responses of *egl-4* and *rgs-3* mutants were best fitted with the first-order (*i.e.*, slow) only model (yellow lines in Fig. 7A and Table 4), suggesting that the fast component of ASH activity requires these gene products. It has been reported that EGL-4 phosphorylates RGS-3, and loss-of-function mutations in either of the genes regulates ASH neuronal and ASH-mediated behavioral responses to other repulsive stimuli (Krzyzanowski et al., 2013). Therefore, this PKG–RGS pathway may regulate the fast component of the ASH response to 2-nonanone as well (see Discussion).

4. Discussion

4.1. 2-nonanone avoidance is enhanced by gain control in ASH sensory neurons

In this study, we demonstrated that the responsiveness of the ASH sensory neurons of *C. elegans* to 2-nonanone exhibits gain control after preexposure to the odor (Fig. 2). Based on the changes in behavioral responsiveness to the odor increase caused by the odor preexposure (Fig. 3A), we consider that this sensory gain control contributes to the ability of *C. elegans* to efficiently navigate down the gradient of repulsive odor. The animals in the 2-nonanone avoidance assay generally move away from the odor source and sense decreases in the odor concentration. However, their avoidance movements are frequently interrupted because of stochastic occurrence of pirouettes and/or of small increases in odor concentration (Yamazoe-Umemoto et al., 2015). This stochastic increase of odor concentration could be caused by (1) the direction of the animals' movement straying from the ideal, (2) small fluctuations in the odor gradient, and/or (3) small periodic changes in the sensed odor concentration caused by the animals' sinusoidal head swing. In the naive and mock-treated conditions, the animals initiate pirouettes when they experience even a small increase in odor concentration (Fig. 3B, top left). However, in the preexposed condition, the animals do not respond to small increases (Fig. 3B, top right) but initiate pirouettes when they sense larger increases (Fig. 3B, bottom panels), which results in a longer avoidance distance traveled in the same period. Thus, experience-dependent changes in ASH response due to gain control likely contribute the enhanced odor avoidance behavior, which could also be effective in a real-world environment infused with noise.

To our knowledge, this is the first report of sensory gain control in wild-type *C. elegans*; sensory gain control has been shown only in a few mutant strains of the animals (Kuhara et al., 2002; Saro et al., 2020). There are multiple examples of behavioral changes in *C. elegans* due to activity changes in sensory neurons that are affected by repeated stimuli, different types of stimuli, or the feeding state (Larsch et al., 2015; Ezcurra et al., 2016; Chew et al., 2018). However, most of them are caused by adaptation or sensitization but not gain control. It is possible that the animals might have developed a special mechanism against 2-nonanone to effectively avoid danger because it is a major volatile compound produced by *P. aeruginosa*, a bacterial species that is pathogenic to *C. elegans* (Labows et al., 1980; Tan et al., 1999; Tan and Ausubel, 2000).

4.2. Estimating the neural mechanism of gain control by mathematical modeling

To obtain quantitative insights into the mechanism of sensory gain control, we performed mathematical modeling. Indeed, mathematical modeling has successfully revealed essential features of the sensory neuronal responses of the animals (Kato et al., 2014; Tanimoto et al., 2017; Itskovits et al., 2018; Ikeda et al., 2021). Our previous pharmacological analysis revealed that ASH activity is composed of fast and

Table 3
Parameter values for Eq. (5).

Fig.	Fig. 6B left	Fig. 6B right			Fig. 7A					
Condition / genotype	Naive	Naive	Mock-treated	Preexp	Wild-type	*osm-9ocr-2*	*tag-180*	*unc-77*	*egl-4*	*rgs-3*
b_1	1.023	1.971	1.581	1.619	0.847	0.419	0.655	0.673	0.643	0.846
b_2	1.268	1.605	1.468	1.619	0.64	0.501	0.712	0.512	0.453	0.706

Parameters b_1 and b_2 were calculated for each set of experiments according to the baseline values.

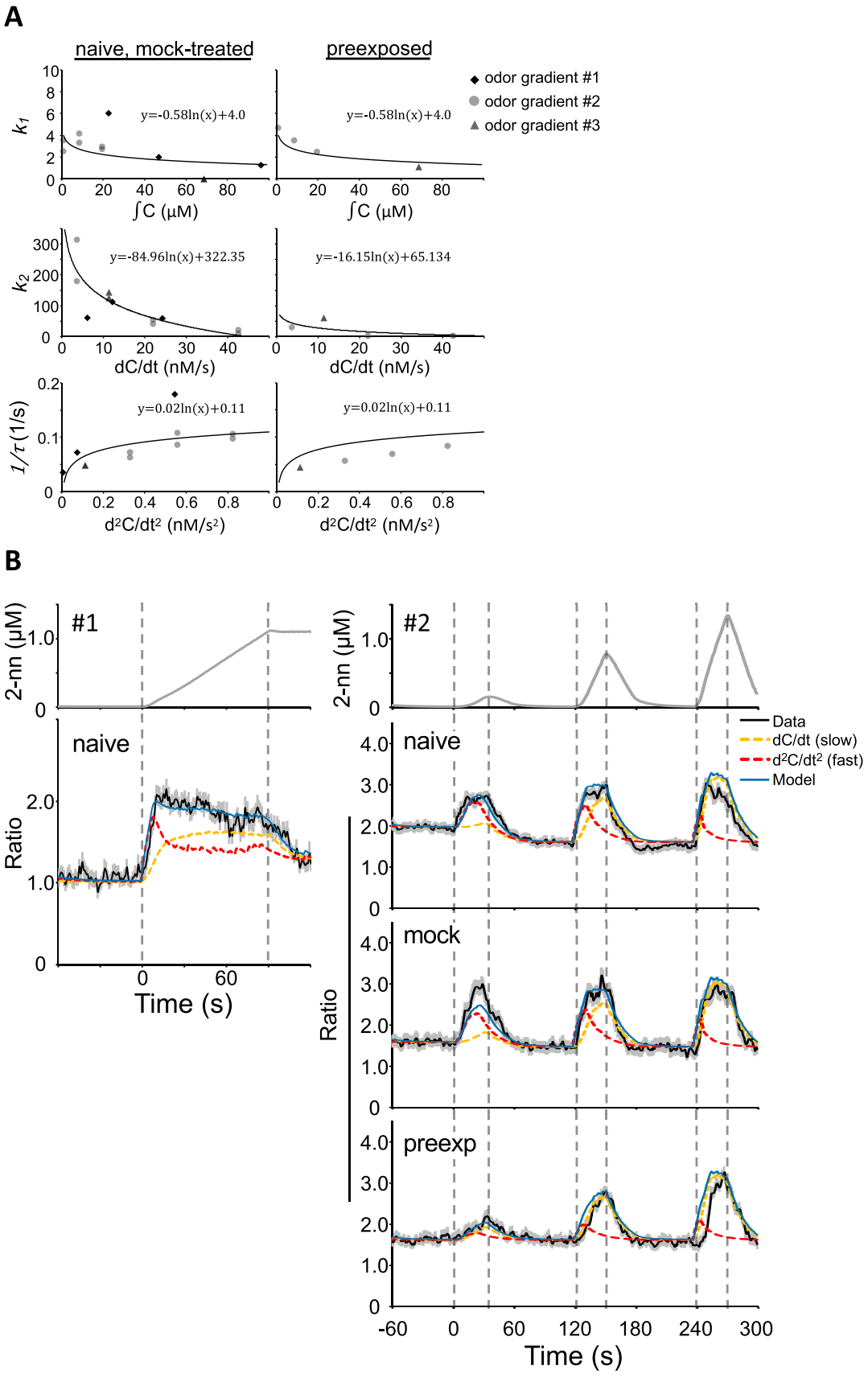

(caption on next page)

Fig. 6. Model of wild-type ASH response fitted to the odor gradient #1 and #2 with stimulus-dependent parameters. **A,** Scatter plots used to find stimulus-dependent parameters for the first and second differential model. Only the parameter of the second-order time-differential, k_2, is substantially different between naive, and mock-treated *versus* preexposed conditions. Black rhombuses, light gray circles, and dark gray triangles represent each ASH response to odor gradient #1, #2, and #3, respectively. Odor gradient #3 was used for the genetic analysis (Fig. 7). **B,** ASH response and its model to a simple odor increase (left; odor gradient #1, same with Fig. 4B left) and to the three consecutive stimuli (right; odor gradient #2, same with Fig. 4B right) with the stimulus-dependent parameters. The black line and the associated gray area are the average ASH responses and their standard errors, the blue line is the model, the yellow and red dashed lines are the first- and second-order components in the model, respectively. The gray dotted line indicates the onset and end of the odor increase phase (For interpretation of the references to color in this figure legend, the reader is referred to the web version of this article).

slow components, and we showed in this study that the fast component can be approximated by a leaky integration of the second-order time--differential of the odor concentration (Fig. 4). Even independent of the pharmacological result, the ASH responses in wild-type animals exhibit overshoot in response to a long-lasting and linearly increasing odor concentration (odor gradient #1 in Fig. 1C, 4 B and 5, and odor gradient #3 in Fig. 7A). More precisely, the response first increases rapidly, and then slowly decreases to a non-zero constant value. The leaky integration of the first-order time-differential of the odor concentration generates a sustained response that converges to a non-zero constant value. The leaky integration of the second-order time-differential generates a rapidly increasing and subsequently decreasing response. Thus, both the pharmacological analysis as well as the analysis of shapes of ASH responses in time domain suggest that the ASH response can be modeled with a leaky integration of the sum of the first- and second-order time-differentials of the odor concentration, and that these two terms well describe essential characteristics of ASH neurons. Indeed, the model had the best goodness of fit in most naive and mock-treated conditions in terms of BIC (Table 1). It should be noted, however, that we only tested the limited kinds of odor gradients, and the equation may not be applicable to ASH responses to every types of odor stimuli; in other words, the fast component could be approximated with another equation such as an alpha function (Rall, 1967). Nevertheless, the leaky integration of the sum of the first- and second-order time-differential equation with stimulus-dependent parameters nicely reproduced the ASH responses, and provided us an important biological insight (see next section). Some details still do not match, suggesting the involvement of other factors in the ASH response.

Remarkably, our model indicates that the preexposure-dependent changes in ASH response can be caused only by the modulation of the fast component (k_2) rather than the modulation of overall ASH response, although the ASH response does exhibit changes in multiple aspects, such as its speed, magnitude, and small increase/decrease when it reaches closes to the maximum value (odor gradient #2 in Fig. 4B). It also explains why ASH responses to a large odor increase are not substantially affected. This result suggests that a specific sensory signaling molecular pathway that suppresses the fast component in ASH neurons is regulated by preexposure to cause experience-dependent modulation of behavior, *i.e.*, learning.

4.3. Relationships between the mathematical model and molecular mechanisms of ASH response

We have previously shown that AWB responses are mediated by EGL-19, an α1 subunit of L-type VGCC, which possesses a long-lasting channel opening property, and that a $G\alpha_o$ homolog, ODR-3, is required for the first-order time-differential of odor concentration (Tanimoto et al., 2017). These results suggest that the constant decrease in 2-nonanone concentration is time-differentiated at the sensory ending by G protein signaling and causes constant depolarization, leading to EGL-19 opening and a continuous influx of calcium into the cells. The slow component in ASH neurons is also mediated by EGL-19 (Tanimoto et al., 2017).

In contrast, the fast component in ASH neurons is likely caused by a transient calcium influx at the onset of odor concentration increase, which ends rapidly (Fig. 4A and 7 B left). One candidate gene product for this was the T-type VGCC ("T" for transient opening) (Nowycky et al., 1985). However, the loss-of-function mutant of the *cca-1* gene, the sole homolog of T-type VGCC in *C. elegans* (Steger et al., 2005), showed wild-type-like ASH responses (Tanimoto et al., 2017). In addition, the results of the loss-of-function mutants of N-type homolog *unc-2* (Tanimoto et al., 2017) and of the homologs of VGCC auxiliary subunit α2δ2 *tag-180* (Fig. 7A) were also wild-type-like responses, suggesting that some other calcium channel(s) may be involved in the fast component.

Still, we found that PKG EGL-4 and RGS RGS-3 possibly modulate the fast component. RGS is known to inhibit G protein signaling to modulate the magnitude and/or time-course of neuronal responses in *C. elegans* and mammals (Cao et al., 2012; Krzyzanowski et al., 2013; Lur and Higley, 2015). In addition, PKG phosphorylates RGS to increase its activity in *C. elegans* and mammals (Huang et al., 2007; Krzyzanowski et al., 2013). Thus, in naive/mock-treated ASH neurons in wild-type animals, the PKG–RGS pathway may inhibit G protein activity that suppresses the ion channel mediating the fast component; in contrast, in the preexposed wild-type and *egl-4* or *rgs-3* animals, the PKG–RGS pathway is inactivated, leading to activation of G protein and inhibition of the channel activity for fast component (Fig. 7B).

While genetic analysis itself would not provide us information related to time-course changes of the gene product activities, the combination with physiological analysis and mathematical modeling provides insights as to how these gene products could affect neural activities dynamically. The characteristics of ASH response were not clear except for the preexposure-dependent gain control aspect, although a simple "first and second differential model" can explain multiple aspects of its differences between with or without preexposure experience, such as the quick rise at the onset of the odor stimulus, the gradual decrease during a long-lasting odor increase, the slow decay during odor decrease (not reproduced by the original simple time-differential model) as well as the gain control (Figs. 4 and 6B). Furthermore, the stimulus-dependent parameters we used in the model may reflect the opening probabilities of the channels for the fast and slow responses, which change according to the intensity of the stimulus. For example, k_1 reduces according to the accumulation of odor concentration (Fig. 6A), which may indicate habituation due to the sustained stimulation from the odor. Further, k_2 reduces according to the average of dC/dt, suggesting that the depolarization level may affect the opening probability because the odor concentration is time-differentiated at the sensory ending and it reflects the depolarization level (Tanimoto et al., 2017). Lastly, $1/\tau$ increases according to the second-order time-differential of odor concentration, which may reflect a change in leakage level at the stimulus onset. Those insights could have not been obtained without the model.

In summary, we showed that gain control occurs in ASH sensory neurons after preexposure to the repulsive odor, and mathematical analysis suggests that this gain control is caused by suppression of the fast component. This gain control likely leads to efficient avoidance behavior that allows the animal to ignore slight increases in odor concentration. In more complex animals, such as mice and *Drosophila*, neurotransmitters such as serotonin or GABA are involved in gain control in peripheral and central sensory systems (Azimi et al., 2020; Olsen and Wilson, 2008) but little is known about their detailed molecular mechanisms. This study may contribute to our understanding of intracellular mechanisms surrounding sensory gain control in animals.

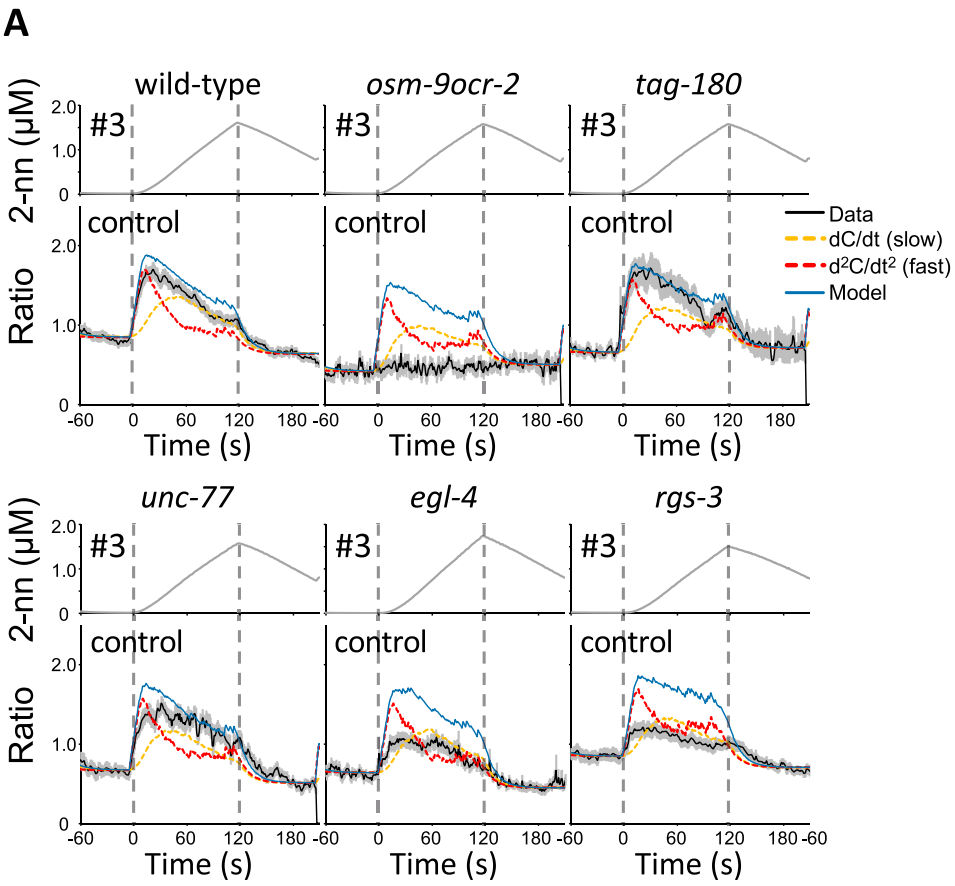

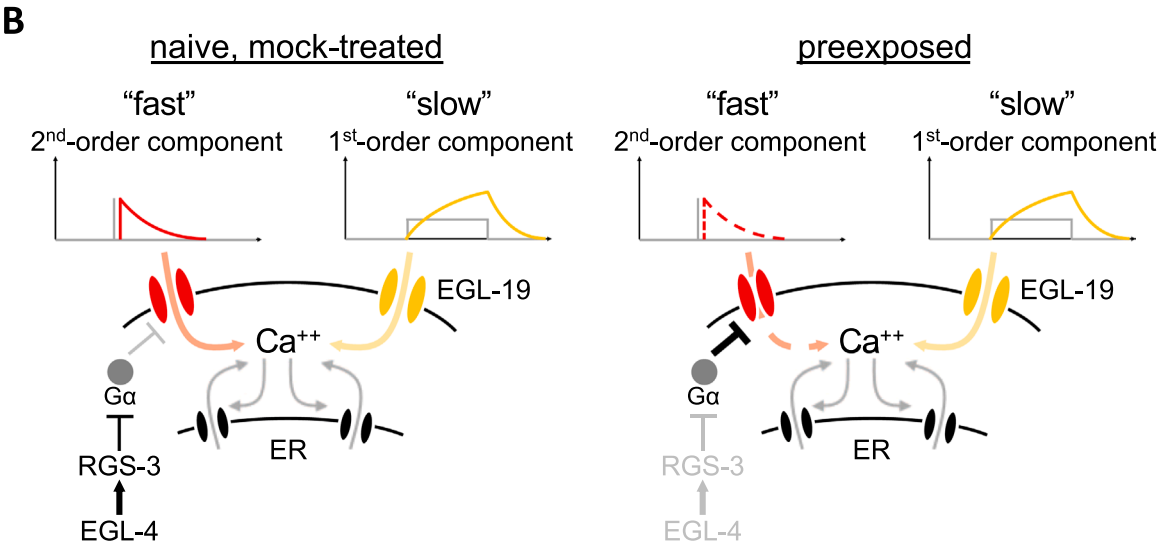

Fig. 7. Genetic analysis of the ASH response. **A,** ASH response in wild-type and mutant animals in control (*i.e.,* naive or mock-treated) condition (n = 51 in wild-type; n = 7 in *osm-9 ocr-2*; n = 15 in *tag-180*; n = 16 in *unc-77*; n = 46 in *egl-4*; n = 29 in *rgs-3*) to a longer and larger continuous odor increase (up to ~2 μM within 120 s; odor gradient #3). We used this odor stimulus with the idea that even milder mutant phenotypes would be observed clearly with a longer and larger stimulus. The black line and the associated gray area are the average ASH responses and their standard errors, respectively. The model parameter $X_e(t)$ was determined in each condition and the other parameters (k_1, k_2 and $1/\tau$) to fit for the wild-type response in Fig. 6 were used, and overlaid with each of the ASH responses. The gray dotted line indicates the onset and end of the odor increase phase. **B,** A proposed molecular model of ASH response. ASH response is mainly mediated by transiently active calcium channels (red) and persistently active L-type VGCCs (yellow). Gα protein activity can suppress the transiently active calcium channels, and this Gα protein activity is inhibited by PKG–RGS pathway in naive/mock-treated conditions. Gain control is caused only by suppression of the transiently active calcium channels *via* the Gα signaling. The calcium influx from the plasma membrane is further increased by the calcium-induced calcium release through IP3 receptor and ryanodine receptor on ER membrane (Tanimoto et al., 2017) (For interpretation of the references to color in this figure legend, the reader is referred to the web version of this article).

Table 4
Summary of BIC value for the ASH model in mutant strains.

Model	N2	*osm-9ocr-2*	*tag-180*	*unc-77*	*egl-4*	*rgs-3*
$\frac{dX}{dt} = k_1\frac{dC}{dt} - \frac{1}{\tau}(X - X_e(t))$	-800.0	**-654.8**	-652.5	-818.6	**-1171**	**-1055**
$\frac{dX}{dt} = k_2\frac{d^2C}{dt^2} - \frac{1}{\tau}(X - X_e(t))$	-768.0	-587.7	-737.4	-795.5	-987.8	-896.7
$\frac{dX}{dt} = k_1\frac{dC}{dt} + k_2\frac{d^2C}{dt^2} - \frac{1}{\tau}(X - X_e(t))$	**-899.7**	-260.2	**-1171**	**-960.8**	-530.4	-454.2

The smallest BIC values under each condition are indicated in bold.

Funding

This study was supported by Japan Society for the Promotion of Science (KAKENHI JP16H06545, 21H02533, 22KK0100 to K.D.K., 17H05968 and 19H04925 to Y.Iwatani), a program for Leading Graduate Schools entitled 'Interdisciplinary graduate school program for systematic understanding of health and disease' (to Y.T., S.J.Y. and Y. E.), Grant-in-Aid for Research in Nagoya City University (48, 1912011, 1921102, 2121101), Toyoaki Scholarship Foundation, and RIKEN Center for Advanced Intelligence Project (to K.D.K).

Competing interests

The authors declare no competing interests.

Data Availability

Main data will be shared through Dryad https://doi.org/10.5061/dryad.37pvmcvmn.

Acknowledgements

We thank Yuki Tsukada, Yuishi Iwasaki, Jared Young, Sakiko Shiga, Masahiro Ueda, and the other Kimura laboratory members for their valuable advice, comments and technical assistance for this study. Nematode strains were provided by the Caenorhabditis Genetics Center (funded by the NIH Office of Research Infrastructure Programs P40 OD010440).

Appendix A. Supporting information

Supplementary data associated with this article can be found in the online version at doi:10.1016/j.neures.2023.01.006.

References

Andersen, R.A., Essick, G.K., Siegel, R.M., 1985. Encoding of spatial location by posterior parietal neurons. Science 230, 456–458. https://doi.org/10.1126/science.4048942.

Anderson, C.T., Kumar, M., Xiong, S., Tzounopoulos, T., 2017. Cell-specific gain modulation by synaptically released zinc in cortical circuits of audition. Elife 6, 1–20. https://doi.org/10.7554/eLife.29893.

Azimi, Z., Barzan, R., Spoida, K., Surdin, T., Wollenweber, P., Mark, M.D., Herlitze, S., Jancke, D., 2020. Separable gain control of ongoing and evoked activity in the visual cortex by serotonergic input. Elife 9, 1–29. https://doi.org/10.7554/eLife.53552.

Bargmann, C.I., 2006. Chemosensation in *C. elegans*. WormBook 1–29. https://doi.org/10.1895/wormbook.1.123.1.

Bargmann, C.I., Hartwieg, E., Horvitz, H.R., 1993. Odorant-selective genes and neurons mediate olfaction in *C. elegans*. Cell 74, 515–527. https://doi.org/10.1016/0092-8674(93)80053-H.

Brenner, S., 1974. The genetics of *Caenorhabditis elegans*. Genetics 77, 71–94. https://doi.org/10.1093/genetics/77.1.71.

Cao, Y., Pahlberg, J., Sarria, I., Kamasawa, N., Sampath, A.P., Martemyanov, K.A., 2012. Regulators of G protein signaling RGS7 and RGS11 determine the onset of the light response in on bipolar neurons. Proc. Natl. Acad. Sci. U. S. A. 109, 7905–7910. https://doi.org/10.1073/pnas.1202332109.

Carew, T.J., Castellucci, V.F., Kandel, E.R., 1971. An analysis of dishabituation and sensitization of the gill-withdrawal reflex in aplysia. Int. J. Neurosci. 2, 79–98. https://doi.org/10.3109/00207457109146995.

Chance, F.S., Abbott, L.F., Reyes, A.D., 2002. Gain modulation from background synaptic input. Neuron 35, 773–782. https://doi.org/10.1016/S0896-6273(02)00820-6.

Chew, Y.L., Tanizawa, Y., Cho, Y., Zhao, B., Yu, A.J., Ardiel, E.L., Rabinowitch, I., Bai, J., Rankin, C.H., Lu, H., Beets, I., Schafer, W.R., 2018. An afferent neuropeptide system transmits mechanosensory signals triggering sensitization and arousal in *C. elegans*. e6 Neuron 99, 1233–1246. https://doi.org/10.1016/j.neuron.2018.08.003.

Colbert, H.A., Smith, T.L., Bargmann, C.I., 1997. OSM-9, a novel protein with structural similarity to channels, is required for olfaction, mechanosensation, and olfactory adaptation in *Caenorhabditis elegans*. J. Neurosci. 17, 8259–8269. https://doi.org/10.1523/jneurosci.17-21-08259.1997.

De Bono, M., Maricq, A.V., 2005. Neuronal substrates of complex behaviors in *C. elegans*. Annu. Rev. Neurosci. 28, 451–501. https://doi.org/10.1146/annurev.neuro.27.070203.144259.

Dragoi, V., Sharma, J., Sur, M., 2000. Adaptation-induced plasticity of orientation tuning in adult visual cortex. Neuron 28, 287–298. https://doi.org/10.1016/S0896-6273(00)00103-3.

Ezcurra, M., Walker, D.S., Beets, I., Swoboda, P., Schafer, W.R., 2016. Neuropeptidergic signaling and active feeding state inhibit nociception in *Caenorhabditis elegans*. J. Neurosci. 36, 3157–3169. https://doi.org/10.1523/JNEUROSCI.1128-15.2016.

Ferkey, D.M., Hyde, R., Haspel, G., Dionne, H.M., Hess, H.A., Suzuki, H., Schafer, W.R., Koelle, M.R., Hart, A.C., 2007. *C. elegans* G Protein Regulator RGS-3 Controls Sensitivity to Sensory Stimuli. Neuron 53, 39–52. https://doi.org/10.1016/j.neuron.2006.11.015.

Ferkey, D.M., Sengupta, P., L'Etoile, N.D., 2021. Chemosensory signal transduction in *Caenorhabditis elegans*. Genetics 217. https://doi.org/10.1093/GENETICS/IYAB004.

Huang, J., Zhou, H., Mahavadi, S., Sriwai, W., Murthy, K.S., 2007. Inhibition of Gαq-dependent PLC-β1 activity by PKG and PKA is mediated by phosphorylation of RGS4 and GRK2. Am. J. Physiol. Cell Physiol. 292, 200–208. https://doi.org/10.1152/ajpcell.00103.2006.

Ikeda, M., Matsumoto, H., Izquierdo, E.J., 2021. Persistent thermal input controls steering behavior in *Caenorhabditis elegans*. PLoS Comput. Biol. 17. https://doi.org/10.1371/JOURNAL.PCBI.1007916.

Itskovits, E., Ruach, R., Kazakov, A., Zaslaver, A., 2018. Concerted pulsatile and graded neural dynamics enables efficient chemotaxis in *C. elegans*. Nat. Commun. 9. https://doi.org/10.1038/s41467-018-05151-2.

Kaplan, J.M., Horvitz, H.R., 1993. A dual mechanosensory and chemosensory neuron in *Caenorhabditis elegans*. Proc. Natl. Acad. Sci. U. S. A. 90, 2227–2231. https://doi.org/10.1073/pnas.90.6.2227.

Kato, S., Xu, Y., Cho, C.E., Abbott, L.F., Bargmann, C.I., 2014. Temporal responses of *C. elegans* chemosensory. Neurons Are Preserv. Behav. Dyn. Neuron 81, 616–628. https://doi.org/10.1016/j.neuron.2013.11.020.

Kimura, K.D., Fujita, K., Katsura, I., 2010. Enhancement of odor avoidance regulated by dopamine signaling in *Caenorhabditis elegans*. J. Neurosci. 30, 16365–16375. https://doi.org/10.1523/JNEUROSCI.6023-09.2010.

Krzyzanowski, M.C., Brueggemann, C., Ezak, M.J., Wood, J.F., Michaels, K.L., Jackson, C. A., Juang, B.T., Collins, K.D., Yu, M.C., L'Etoile, N.D., Ferkey, D.M., 2013. The *C. elegans* cGMP-dependent protein kinase EGL-4 regulates nociceptive behavioral sensitivity. PLoS Genet 9. https://doi.org/10.1371/journal.pgen.1003619.

Kuhara, A., Inada, H., Katsura, I., Mori, I., 2002. Negative regulation and gain control of sensory. Neurons *C. elegans* calcineurin TAX-6. Neuron 33, 751–763. https://doi.org/10.1016/S0896-6273(02)00607-4.

Kwok, T.C.Y., Ricker, N., Fraser, R., Chan, A.W., Burns, A., Stanley, E.F., McCourt, P., Cutler, S.R., Roy, P.J., 2006. A small-molecule screen in *C. elegans* yields a new calcium channel antagonist. Nature 441, 91–95. https://doi.org/10.1038/nature04657.

L'Etoile, N.D., Coburn, C.M., Eastham, J., Kistler, A., Gallegos, G., Bargmann, C.I., 2002. The cyclic GMP-dependent protein kinase EGL-4 regulates olfactory adaptation in *C. elegans*. Neuron 36, 1079–1089. https://doi.org/10.1016/S0896-6273(02)01066-8.

Labows, J.N., McGinley, K.J., Webster, G.F., Leyden, J.J., 1980. Headspace analysis of volatile metabolites of Pseudomonas aeruginosa and related species by gas chromatography-mass spectrometry. J. Clin. Microbiol. 12, 521–526. https://doi.org/10.1128/jcm.12.4.521-526.1980.

Lainé, V., Frøkjær-Jensen, C., Couchoux, H., Jospin, M., 2011. The α1 subunit EGL-19, the α2/δ subunit UNC-36, and the β subunit CCB-1 underlie voltage-dependent calcium currents in *Caenorhabditis elegans* striated muscle. J. Biol. Chem. 286, 36180–36187. https://doi.org/10.1074/jbc.M111.256149.

Larsch, J., Flavell, S.W., Liu, Q., Gordus, A., Albrecht, D.R., Bargmann, C.I., 2015. A Circuit for Gradient Climbing in *C. elegans* Chemotaxis. Cell Rep. 12, 1748–1760. https://doi.org/10.1016/j.celrep.2015.08.032.

Lewis, J.A., Wu, C.H., Berg, H., Levine, J.H., 1980. The genetics of levamisole resistance in the nematode *Caenorhabditis elegans*. Genetics 95, 905–928. https://doi.org/10.1093/genetics/95.4.905.

Lur, G., Higley, M.J., 2015. Glutamate receptor modulation is restricted to synaptic microdomains. Cell Rep. 12, 326–334. https://doi.org/10.1016/j.celrep.2015.06.029.

Nowycky, M.C., Fox, A.P., Tsien, R.W., 1985. Three types of neuronal calcium channel with different calcium agonist sensitivity. Nature 316, 440–443. https://doi.org/10.1038/316440a0.

Ohzawa, I., Sclar, G., Freeman, R.D., 1982. Contrast gain control in the cat visual cortex. Nature 298, 266–268. https://doi.org/10.1038/298266a0.
Olsen, S.R., Wilson, R.I., 2008. Lateral presynaptic inhibition mediates gain control in an olfactory circuit. Nature 452, 956–960. https://doi.org/10.1038/nature06864.
Pierce-Shimomura, J.T., Morse, T.M., Lockery, S.R., 1999. The fundamental role of pirouettes in *Caenorhabditis elegans* chemotaxis. J. Neurosci. 19, 9557–9569. https://doi.org/10.1523/jneurosci.19-21-09557.1999.
Priebe, N.J., Ferster, D., 2002. A new mechanism for neuronal gain control (or how the gain in brains has mainly been explained. Neuron 35, 602–604. https://doi.org/10.1016/S0896-6273(02)00829-2.
Rall, W., 1967. Distinguishing theoretical synaptic potentials computed for different soma-dendritic distributions of synaptic. J. Neurophysiol. 5, 1138–1168. https://doi.org/10.1152/jn.1967.30.5.1138.
Root, C.M., Masuyama, K., Green, D.S., Enell, L.E., Nässel, D.R., Lee, C.H., Wang, J.W., 2008. A presynaptic gain control mechanism fine-tunes olfactory behavior. Neuron 59, 311–321. https://doi.org/10.1016/j.neuron.2008.07.003.
Saro, G., Lia, A.S., Thapliyal, S., Marques, F., Busch, K.E., Glauser, D.A., 2020. Specific ion channels control sensory gain, sensitivity, and kinetics in a tonic thermonociceptor. e4 Cell Rep. 30, 397–408. https://doi.org/10.1016/j.celrep.2019.12.029.
Sasakura, H., Mori, I., 2013. Behavioral plasticity, learning, and memory in *C. elegans*. Curr. Opin. Neurobiol. 23, 92–99. https://doi.org/10.1016/j.conb.2012.09.005.
Schwarz, G., 1978. Estimating the dimension of a model. Ann. Stat. 6, 461–464. https://doi.org/10.1214/aos/1176344136.
Shaner, N.C., Campbell, R.E., Steinbach, P.A., Giepmans, B.N.G., Palmer, A.E., Tsien, R.Y., 2004. Improved monomeric red, orange and yellow fluorescent proteins derived from Discosoma sp. red fluorescent protein. Nat. Biotechnol. 22, 1567–1572. https://doi.org/10.1038/nbt1037.
Shapley, R., Enroth-Cugell, C., 1984. Visual adaptation and retinal gain controls. Eng. Sci. 3, 263–346. https://doi.org/10.1016/0278-4327(84)90011-7.
Steger, K.A., Shtonda, B.B., Thacker, C., Snutch, T.P., Avery, L., 2005. The *C. elegans* T-type calcium channel CCA-1 boosts neuromuscular transmission. J. Exp. Biol. 208, 2191–2203. https://doi.org/10.1242/jeb.01616.
Tan, M.W., Ausubel, F.M., 2000. *Caenorhabditis elegans*: a model genetic host to study Pseudomonas aeruginosa pathogenesis. Curr. Opin. Microbiol 3, 29–34. https://doi.org/10.1016/S1369-5274(99)00047-8.
Tan, M.W., Mahajan-Miklos, S., Ausubel, F.M., 1999. Killing of *Caenorhabditis elegans* by Pseudomonas aeruginosa used to model mammalian bacterial pathogenesis. Proc. Natl. Acad. Sci. U. S. A. 96, 715–720. https://doi.org/10.1073/pnas.96.2.715.
Tanimoto, Y., Kimura, K.D., 2021. Calcium imaging of neuronal activity under gradually changing odor stimulation in *Caenorhabditis elegans*. Bio-Protoc. 11, 1–23. https://doi.org/10.21769/bioprotoc.3866.
Tanimoto, Y., Yamazoe-Umemoto, A., Fujita, K., Kawazoe, Y., Miyanishi, Y., Yamazaki, S.J., Fei, X., Busch, K.E., Gengyo-Ando, K., Nakai, J., Iino, Y., Iwasaki, Y., Hashimoto, K., Kimura, K.D., 2017. Calcium dynamics regulating the timing of decision-making in *C. elegans*. Elife 6, 1–30. https://doi.org/10.7554/eLife.21629.
Tian, L., Hires, S.A., Mao, T., Huber, D., Chiappe, M.E., Chalasani, S.H., Petreanu, L., Akerboom, J., McKinney, S.A., Schreiter, E.R., Bargmann, C.I., Jayaraman, V., Svoboda, K., Looger, L.L., 2009. Imaging neural activity in worms, flies and mice with improved GCaMP calcium indicators. Nat. Methods 6, 875–881. https://doi.org/10.1038/nmeth.1398.
Tobin, D.M., Madsen, D.M., Kahn-Kirby, A., Peckol, E.L., Moulder, G., Barstead, R., Maricq, A.V., Bargmann, C.I., 2002. Combinatorial expression of TRPV channel proteins defines their sensory functions and subcellular localization in *C. elegans*. neurons. Neuron 35, 307–318. https://doi.org/10.1016/S0896-6273(02)00757-2.
Ulanovsky, N., Las, L., Nelken, I., 2003. Processing of low-probability sounds by cortical neurons. Nat. Neurosci. 6, 391–398. https://doi.org/10.1038/nn1032.
Woolf, C.J., Ma, Q., 2007. Nociceptors-noxious stimulus detectors. Neuron 55, 353–364. https://doi.org/10.1016/j.neuron.2007.07.016.
Yamazaki, S.J., Ohara, K., Ito, K., Kokubun, N., Kitanishi, T., Takaichi, D., Yamada, Y., Ikejiri, Y., Hiramatsu, F., Fujita, K., Tanimoto, Y., Yamazoe-Umemoto, A., Hashimoto, K., Sato, K., Yoda, K., Takahashi, A., Ishikawa, Y., Kamikouchi, A., Hiryu, S., Maekawa, T., Kimura, K.D., 2019. STEFTR: A hybrid versatile method for state estimation and feature extraction from the trajectory of animal behavior. Front. Neurosci. 13. https://doi.org/10.3389/fnins.2019.00626.
Yamazoe-Umemoto, A., Fujita, K., Iino, Y., Iwasaki, Y., Kimura, K.D., 2015. Modulation of different behavioral components by neuropeptide and dopamine signalings in non-associative odor learning of *Caenorhabditis elegans*. Neurosci. Res. 99, 22–33. https://doi.org/10.1016/j.neures.2015.05.009.
Yeh, E., Ng, S., Zhang, M., Bouhours, M., Wang, Y., Wang, M., Hung, W., Aoyagi, K., Melnik-Martinez, K., Li, M., Liu, F., Schafer, W.R., Zhen, M., 2008. A putative cation channel, NCA-1, and a novel protein, UNC-80, transmit neuronal activity in *C. elegans*. PLoS Biol. 6, 0552–0567. https://doi.org/10.1371/journal.pbio.0060055.
Yemini, E., Jucikas, T., Grundy, L.J., Brown, A.E.X., Schafer, W.R., 2013. A database of *Caenorhabditis elegans* behavioral phenotypes. Nat. Methods 10, 877–879. https://doi.org/10.1038/nmeth.2560.